Available online at www.sciencedirect.com
SCIENCE DIRECT®
Journal of Power Sources 125 (2004) 1–9
JOURNAL OF POWER SOURCES
www.elsevier.com/locate/jpowsour

Novel method for investigation of two-phase flow in liquid feed direct methanol fuel cells using an aqueous H_2O_2 solution

T. Bewer, T. Beckmann, H. Dohle*, J. Mergel, D. Stolten

Forschungszentrum Jülich GmbH, Institut für Werkstoffe und Verfahren der Energietechnik (IWV3), D 52425 Jülich, Germany

Received 16 April 2003; received in revised form 1 July 2003; accepted 3 July 2003

Abstract

One major issue in the development of direct methanol fuel cells (DMFC) is the management of the evolving CO_2 gas bubbles in the flow fields. These bubbles influence the flow distribution and therefore the power density of a cell. In this paper, a novel method for in situ production of bubbles in a test cell made of perspex is presented. The method is based on the decomposition of hydrogen peroxide solution (H_2O_2) to oxygen and water in aqueous media at the presence of a catalyst. By using an appropriate H_2O_2-concentration, the gas evolution rate can be set to same order of magnitude as in real direct methanol fuel cells. This approach allows the simulation of the flow distribution in DMFC by simple low-cost hardware. As no current conducting parts are needed, the whole dummy cell can be made of perspex to ensure a complete visibility of the flow.

In a perspex flow cell with an active area of 600 cm^2, the flow homogeneity as a function of gas evolution rate, flow field and manifold design was investigated. Experiments show that splayed manifolds have a superior performance concerning flow uniformity compared to other designs. The use of grid structures as a flow field gives good bubble transport at all investigated current densities.

Keywords: DMFC; Two-phase flow; Flow-field design; Manifold design

1. Introduction

Fuel cells are promising energy converters since the efficiency achievable is higher than in power plants or internal combustion engines [1]. In particular, PEM and direct methanol fuel cells (DMFC) fuel cells are interesting for automotive and portable applications because of their low operating temperature. DMFC stacks in the power range of 500 W to 1 kW have recently been reported [2,3].

In the low temperature range, DMFCs are operated with a liquid water/methanol mixture. The cathode is fed with oxygen or air. In a direct methanol fuel cell, the following catalytically activated reactions take place:

anode : $CH_3OH + H_2O \Rightarrow CO_2 + 6H^+ + 6e^-$

cathode : $6H^+ + 6e^- + 1.5O_2 \Rightarrow 3H_2O$

over all reaction : $CH_3OH + 1.5O_2 \Rightarrow CO_2 + 2H_2O$

One of the main problems of the DMFC is the multistage nature of the anodic reaction. In DMFCs, CO or COH occurs as a stable, adsorbed intermediate of methanol oxidation [4]. Poisoning of the anode catalysts by these adsorbates leads to considerable anodic overpotentials. The methanol oxidation takes place through a reaction with adsorbed OH, which is the rate determining step [5]. Both the performance and the efficiency of a DMFC are strongly influenced by the methanol concentration. Using a methanol leaky membrane like Nafion, the methanol concentration influences in general both anode potential and cathode potential. Typical methanol concentrations are in the range from 0.1 to 1 M depending on the operating conditions as current, temperature and pressure. In this concentration range, the water activity which is important for the oxidation kinetics is nearly constant, so that the changes in the electrode potentials are dominated by the methanol concentration. Too low a methanol concentration is mainly accompanied by methanol depletion in the anode catalyst layer causing voltage losses due to diffusion overpotentials [6]. If the methanol concentration is too high methanol permeates to the cathode where it is oxidised to CO_2 and water. In addition, the cell voltage is

* Corresponding author. Fax: +49-2461-6695.
E-mail address: h.dohle@fz-juelich.de (H. Dohle).

0378-7753/$ – see front matter © 2003 Elsevier B.V. All rights reserved.
doi:10.1016/S0378-7753(03)00824-3

lowered by the formation of a mixed potential at the cathode. Therefore, the local methanol concentration in a cell must be kept at an optimum level. The flow distribution across the whole cell area must be as homogeneous as possible to prevent fractions of the cell area to be depleted caused by insufficient supply of methanol. The effects of methanol concentration on the methanol permeation and on both the anode and the cathode potential has been described in detail in [6]. In addition, an pressure drop as low as possible is required, since a low pressure drop reduces the parasitic power demand of peripherical components like pumps and compressors [7].

The reactants can be distributed on the active area of the fuel cell by different flow-field structures. Usually grid [8], channel [9], meander [10] structures and metal screens [11] are utilised as a flow field in DMFC and PEFC cells. Channel and grid structures have been investigated in single-phase flow showing good flow distribution at low pressure drops [12].

In fuel cell operation, a two-phase flow in the anode and the cathode compartment is predominant. On the cathode liquid water is present in the gas stream. Therefore, flooding of certain cell areas can occur, which leads to reduced cell performance [13]. Consequently, the used flow field has to discharge the liquid water properly.

On the anode, the CO_2 production in the aqueous medium leads to bubble formation. These bubbles influence the flow distribution in the anodic flow compartment and therefore the local methanol concentration and performance. The flow distribution depends strongly on the geometry, the current density and the flow rate of the reactants.

Previous investigations of Scott et al. [14] concerning the gas management in the anode compartment were performed in working cells with transparent bipolar plates. These investigations showed that channel structures were blocked by bubbles at low mass flows. Higher fluid velocities at higher mass flows can remove this blockages. An analysis of the influence of mesh size on the bubble discharge indicated that some metal meshes are proper for fuel cell operation [11].

These investigations are limited by ohmic losses in the laterally conducting mesh. Hence, we developed a novel method to analyse the interaction of the flow distribution and the bubble-generation in an aqueous medium [15]. The method is based on the decomposition of hydrogen peroxide solution (H_2O_2) to oxygen and water in aqueous media at the presence of a catalyst. By using an appropriate H_2O_2-concentration, the gas evolution rate can be set to same order of magnitude as in real direct methanol fuel cells. Consequently, the bubble formation in the anode compartment of a DMFC without any electrical current can be simulated. The current density to be simulated can be adjusted by an appropriate setting of the H_2O_2-concentration independently of ohmic losses. Using a perspex flow cell, the flow can be completely visualised. This cell has a simple modular design in which different manifold and flow-fields can be tested.

2. Experimental

2.1. Test rig

Fig. 1 gives the schematic set-up of the test rig. A gear pump transports peroxide solution from a liquid reservoir via the test cell either back into the reservoir or alternatively to the outlet. A manometer measures the pressure drop in the test cell. A digital camera takes 10 pictures per second of the flow plate, which are then digitally evaluated by the computer.

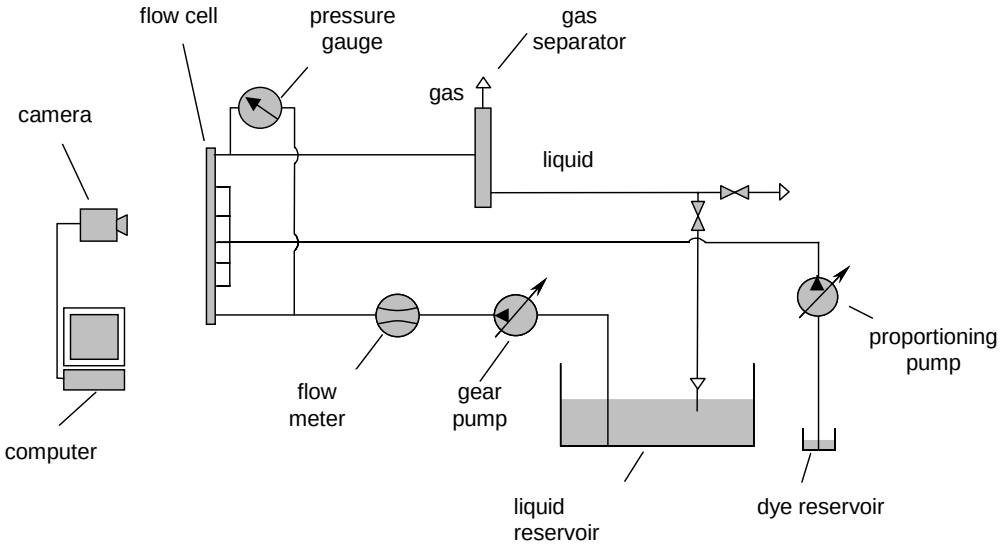

Fig. 1. Schematic set-up of the test rig.

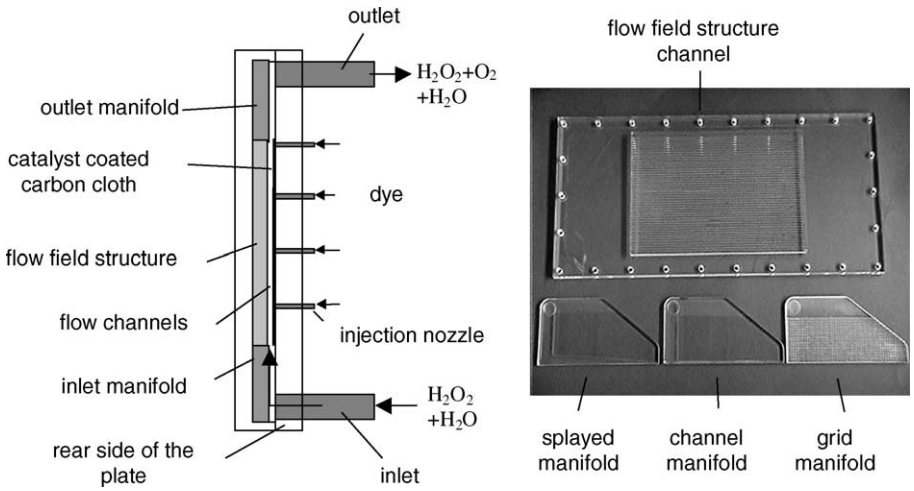

Fig. 2. Left: basic principle of two-phase flow investigations. Right: examples of flow fields and manifolds analysed.

The gas volume arising in the flow cell is measured by a gas separator. The remaining liquid containing H_2O_2 is re-circulated to the reservoir. This is important with regard to the O_2-saturation of the liquid. The saturation prevents additional oxygen from being dissolved in the liquid phase instead of forming bubbles.

In order to visualise the water flow, dye dissolved in de-ionised water can be injected into the water flow from a dye reservoir.

2.2. Flow cell

Fig. 2 shows the principle of the two-phase flow investigations in the flow cell. The flow cell consists of different modules as flow fields or different manifolds. Small injection nozzles for the dye injection are located on the rear side. The catalyst coated carbon cloth is located between the flow profile and rear of the plate.

2.2.1. Preparation of the catalyst coated carbon cloth

A carbon cloth was pre-treated by spraying a mixture of carbon black (XC72) and PTFE (5–10% PTFE) with a loading of approximately 5 mg/cm^2. Afterwards, a catalyst layer is sprayed on the pre-treated cloth. As a catalyst for the decomposition of H_2O_2 PtRu on XC72 (catalyst wt.% 40%) with an atomic ratio of 1:1 was used. The total catalyst loading was 4 mg/cm^2. To ensure good mechanical properties Nafion solution with an amount of 20 w% was added as a binder.

2.3. Simulation of current density: principle of gas formation

In the investigation of two-phase flow, an aqueous hydrogen peroxide solution is used as substitute for the methanol/water mixture. It is fed into the compartment of the test cell representing the anode compartment of the real fuel cell. A catalyst coated carbon cloth is used to decompose the hydrogen peroxide.

2.3.1. Adjusting the H_2O_2-concentration

The H_2O_2 is decomposed into water and oxygen in presence of the PtRu-catalyst. The reaction rate depends on the temperature and on the concentration. As in the experiments, the temperature was set constantly to 30 °C, the concentration is used as the single parameter to adjust the gas evolution.

By varying the H_2O_2-concentration, current densities in a wide range can be simulated. As in real DMFC, current generation is accompanied by CO_2 production, the gas generation in the dummy cell can be recalculated to a corresponding current density of a real DMFC using Faraday's law. The quantity of the gas produced in the dummy cell is determined in a gas separator and the recalculated accordingly

$$i_{\mathrm{eq}} = \frac{1}{A_{\mathrm{cell}}} \frac{\dot{V}_{\mathrm{gas}}}{v_{\mathrm{M}}} 6F \tag{2.1}$$

with A_{cell} being the cell area, F representing Faraday's constant (96,485 As/mol) and $\dot{V}_{\mathrm{gas}}$ the measured gas evolution. The constant $v_{\mathrm{M}} = 24{,}412\,\mathrm{cm}^3/\mathrm{mol}$ is needed to transfer the volume flow into a molar flow (specific molar volume). Eq. (2.1) assumes that the whole amount of produced CO_2 in real DMFC leads to bubble formation and that none of the CO_2 is solved in the water/methanol mixture without bubble formation. This assumption is justified as in a liquid operated DMFC, the anode water/methanol mixture is at least after a few minutes of operation saturated with CO_2. Once the methanol/water loop is saturated, additional CO_2 produced at the anode can only be released as gas bubbles.

Furthermore, the gas evolution depends on the geometry of the flow field as shown in Table 1. The necessary H_2O_2-concentration to produce a specific flow of gas bubbles (expressed according to Eq. (2.1) as an equivalent

Table 1
H_2O_2-concentration for different flow fields to simulate DMFC current densities

Flow field		H_2O_2-concentration (vol.%) at 10 l/h		H_2O_2-concentration (vol.%) at 20 l/h		H_2O_2-concentration (vol.%) at 30 l/h	
Channel (mm)	Rib (mm)	100 (mA/cm^2)	500 (mA/cm^2)	100 (mA/cm^2)	500 (mA/cm^2)	100 (mA/cm^2)	500 (mA/cm^2)
1	3	2.04	6.12	2.51	6.12	2.70	6.05
2	2	2.05	6.21	1.95	6.10	1.87	5.61
3	1	1.25	3.4	1.23	3.35	1.19	3.32

The flow of the water/H_2O_2 mixture was varied from 10 to 30 l/h.

current density for DMFC) is the lowest for the widest channel width of 3 mm. Smaller channels seem to cause mass transport problems of H_2O_2, towards the active reaction zones especially beneath the ribs.

The volume flow of the methanol/water mixture in real DMFC can be calculated using Faraday's law:

$$\dot{V} = \frac{I}{6F}\frac{1}{c_{\mathrm{MeOH}}}\lambda_{\mathrm{MeOH}}\frac{m^3}{1000l} \tag{2.2}$$

with c_{MeOH} being the molar concentration and λ_{MeOH} being the stoichiometric flow rate. It is a theoretically derived equation.

For the experiments in the test cell, the volume flow calculated according Eq. (2.2) was adjusted. Typical ranges for the flow rate λ_{MeOH} are from 5 to 20 depending on the methanol concentration and the power density (Table 2). Higher power outputs are accompanied with higher stoichiometric flow rates to ensure on the one hand a sufficient supply of reactants to the whole area of the cell and on the other hand, a sufficient removal of the process heat.

2.4. Analysed structures

2.4.1. Flow-field designs

Among the various possible flow field described above, the interest was concentrated on the grid and parallel channel structures. These flow field offer low pressure drops due to the relatively low flow velocity compared to, e.g. meander structures. Low pressure drops are an important criterion for large size flow fields (600 cm^2) as they reduce the energy demand of auxiliary system components as pumps or compressors.

Of particular interest is the behaviour of these structures with respect to their tendency to become clogged by gas bubbles and the influence of the bubble formation on the overall flow homogeneity. The structures analysed are listed in Table 3.

The structures were in all cases manufactured of perspex and designed as a single part to be inlaid in the modular test cell (Fig. 2).

2.4.2. Manifold designs to be investigated

Another focus of the flow analysis is the influence of the manifold design. Three basic manifold structures are investigated (Table 4):

- rectangular channel;
- splayed channel;
- grid structure.

By the modular test cell (Fig. 2), these manifold structures can be combined with the different flow fields.

Important variation parameters for channel manifolds are channel diameter and channel geometry. Wide manifolds are advantageous in terms of pressure drop. With respect to compact dimensions and thus greater power density, small manifold widths are to be preferred. A further distinction is made between splayed and straight channel manifolds. Since the volumetric flow decreases continuously, the cross-section must also be reduced so that a constant speed can be maintained in the splayed manifold.

Analogously to the grid distributors, manifolds with grid structures are in principle very well suited for a homogeneous distribution of the two-phase mixture with a low pressure drop and an effective transportation of bubbles in the manifold region [14]. For reasons of completeness, these structures are experimentally evaluated and compared to other manifold designs.

A qualitative rate determination is performed for each flow structure. The flow is analysed visually and divided into zones of large and small flow rate and into homogeneous and stagnant bubble discharge.

Table 2
Conditions for the flow experiments

Active area (cm^2)	600 (= 20 × 30)
Simulated current density, i (mA/cm^2)	100–500
Simulated current, I (A)	60–300
Molar concentration of the methanol solution to be simulated (M)	1
Stoichiometric flow rate, λ_{MeOH}	5–20
Volumetric flow (l/h)	2–40

3. Experimental results

3.1. Influence of the flow-field structures on the bubble formation and on the flow homogeneity

The experimental set-up served for both the variation of the flow field and the manifold.

Table 3
Experimentally tested flow field design

Flow-field design	Channel height (mm)	Open cross surface area (−)	Structure (scheme)
Channel (2 mm), rib (2 mm)	2	0.5	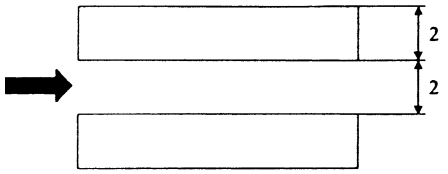
Channel (1 mm), rib (3 mm)	2	0.25	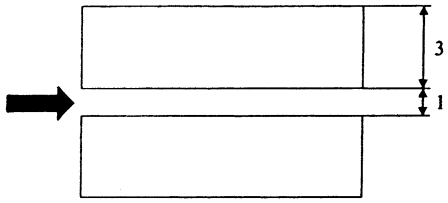
Channel (3 mm), rib (1 mm)	2	0.75	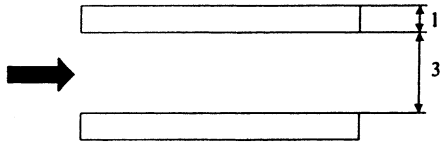
Grid (2 mm)	2	0.75	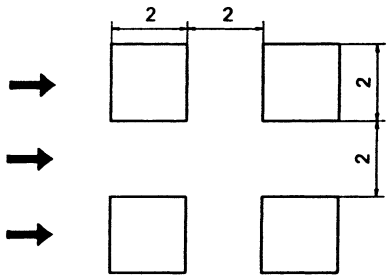

The channel height of 2 mm is constant in all cases. The flow field area is 600 cm^2 (width 20 cm, length 30 cm).

Table 4
Manifold structures analysed

Type of manifold	Structure
Channel: (a) width 8.3 (mm); (b) width 3 (mm)	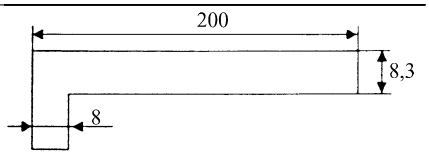
Splayed channel	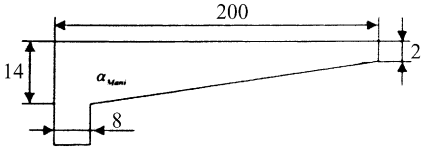
Grid manifold	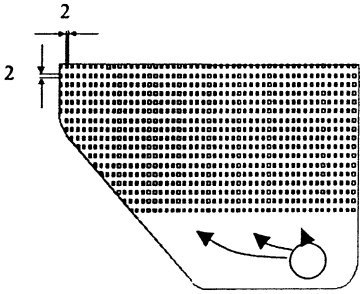

First, the channel structure and the grid structure described in Table 3 have been compared using a rectangular manifold design. General observations concerning the bubble formation and the bubble discharge are made.

Then, in continuation, the flow homogeneity in the respective structures was investigated qualitatively. In addition to the flow-field evaluation, the experimental set-up gives an detailed view on the process of gas evolution beginning at the gas diffusion layer. Tiny gas bubbles are produced which adhere on the gas diffusion layer because of their small size. Once grown to a critical size, they become detached and flow upwards joining together to form larger bubble structures. These processes are described in the following for different flow fields and manifold structures.

3.1.1. Bubble formation and discharge in channel and grid structures

3.1.1.1. Channel structure. Fig. 3 shows as an example the result of the analysis for a channel structure. The liquid and bubbles flow upwards at the same velocity which has been proven by adding white ink into the flow channel.

The bubble size in the channels depends on the flow rate. When a bubble reaches a critical diameter then the force

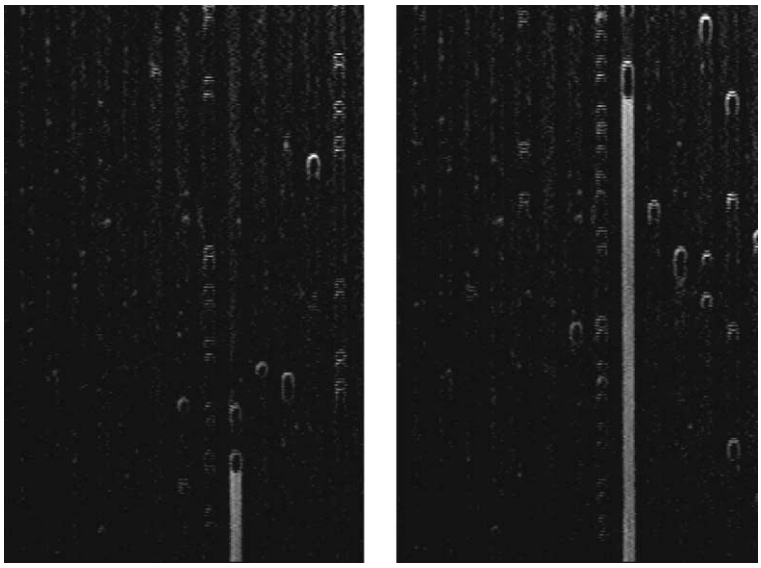

Fig. 3. Visualised two-phase flow in a channel structure. The visualisation has been effected by injection of white ink into a single channel.

of adhesion is equal to the force acting due to the flow. In relation to their volume, small bubbles develop higher adhesion forces. Therefore, higher flow rates consequently lead to smaller bubbles. In the following, two different flow types are distinguished:

- stagnant flow and stagnant bubble discharge;
- homogeneous flow.

The case of stagnant flow generally only occurs the parts of the flow field where the flow velocity is slow either due to the operating conditions or the geometry of the flow field. In some of the channels affected, the velocity may decrease to zero. Gas then collects there so that one or more large gas bubbles form in the channel and are released randomly.

The pressure drop in the flow structure Δp is composed of the hydrostatic pressure and the friction losses. Due to their surface tension, stagnant gas bubbles increase the friction losses. Once a channel is blocked by a bubble, the flow through the neighbour channels increases.

The second flow type is the homogeneous flow with a homogeneous bubble discharge. In experimental channel structures, the bubbles reach a maximum length of 2–3 cm inside the channels. This type of flow is characterised by the absence of an accumulation of bubbles in the cell.

3.1.1.2. Grid structure. The flow behaviour of the grid structure differs fundamentally from that of the channel

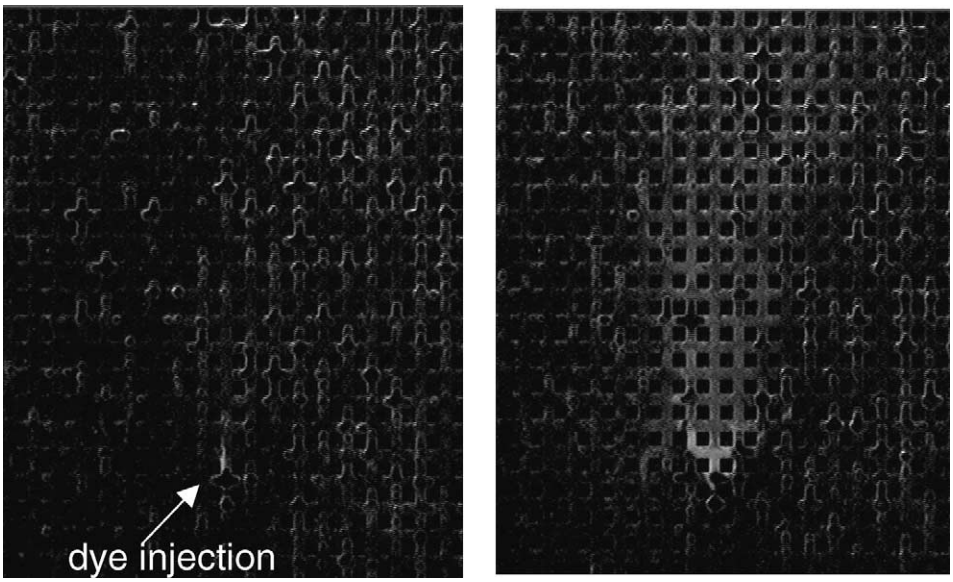

Fig. 4. Visualised two-phase flow in a grid structure left: beginning of dye injection right: dye distribution in the flow field.

structure. In addition to the vertical *y*-component, the flow media here are also able to use the horizontal *x*-component as the flow direction.

In the experiments, it was found that the gas bubbles rise exclusively in a vertical direction also in areas where the liquid phase of the flow has horizontal fractions. With regard to agglomeration of bubbles this effect is less pronounced compared to channel structures. Typical maximum bubble sizes are about 0.2–0.5 cm. These bubbles are discharged homogeneously by the liquid flow phase.

In contrast to the gas flow, the liquid flow has a horizontal component. As for the channel structure, this was determined by visualising the liquid using a white dye. As can be seen from Fig. 4, the gas and the liquid have a velocity relative to each other. The vertical path is frequently blocked by the volume of gas bubbles which increases the flow resistance, respectively, the pressure drag factor of the flow field.

3.1.2. Analysis of flow homogeneity for the variation of flow fields

In the diagrams, the bubble velocity w/w_m is plotted against the plate width x. For reasons of simplification it is normalised to the mean bubble velocity.

Irrespective of the current density, the volumetric flows and the manifolds the two-phase flow in the grid structure always displays homogeneous bubble transport. The bubbles have a uniform velocity at each location.

Furthermore, the three different channel profiles will be discussed. In this analysis, the same boundary conditions hold for all the structures. The 8.3 mm manifold channel serves as the basis. A volumetric flow of 30 l/h is investigated at simulated current densities of $i = 500\,\mathrm{mA/cm^2}$. The experimentally determined distributions are shown in Fig. 5.

With the channel profiles, the greatest flow problems under the given conditions occur in the region of the manifold inlets and outlets. The inflow into the inlet manifold in the region of $x = 0$–25 mm causes a stagnation pressure which locally influences the pressure profile. The reverse effect occurs in the outlet manifold in the region of $x =$ 175–200 mm. A reduction in pressure is caused here due to the low back-pressure of the outlet. In comparison to the middle region, a small pressure difference Δp between the manifolds prevails in the boundary area thus leading to a low flow rate. The velocity profile therefore makes an inhomogeneous impression. At a current density of $i = 100\,\mathrm{mA/cm^2}$, this influence is better compensated by the wide channel structures than by the narrow ones. In this case, the velocity gradients across the plate width *x* are smaller.

At larger current densities ($i = 500\,\mathrm{mA/cm^2}$, 30 l/h) this effect is reversed. The velocity profiles of the narrow channels are moderated by the pressure profile in the manifold, whereas the wide channels are negatively influenced. At a current density of $i = 500\,\mathrm{mA/cm^2}$, the bubble discharge is poor for all channel structures. If the flow rate is increased than this increases the liquid fraction of the flow and causes a greater pressure difference across the plate. This thus reduces the bubble influence and enables a more homogeneous bubble discharge.

The observations suggest that in addition to the flow rate in the channels, the gas management of the manifold is the decisive factor influencing the flow distribution of two-phase flow. Compared to that, the channel width is of minor significance.

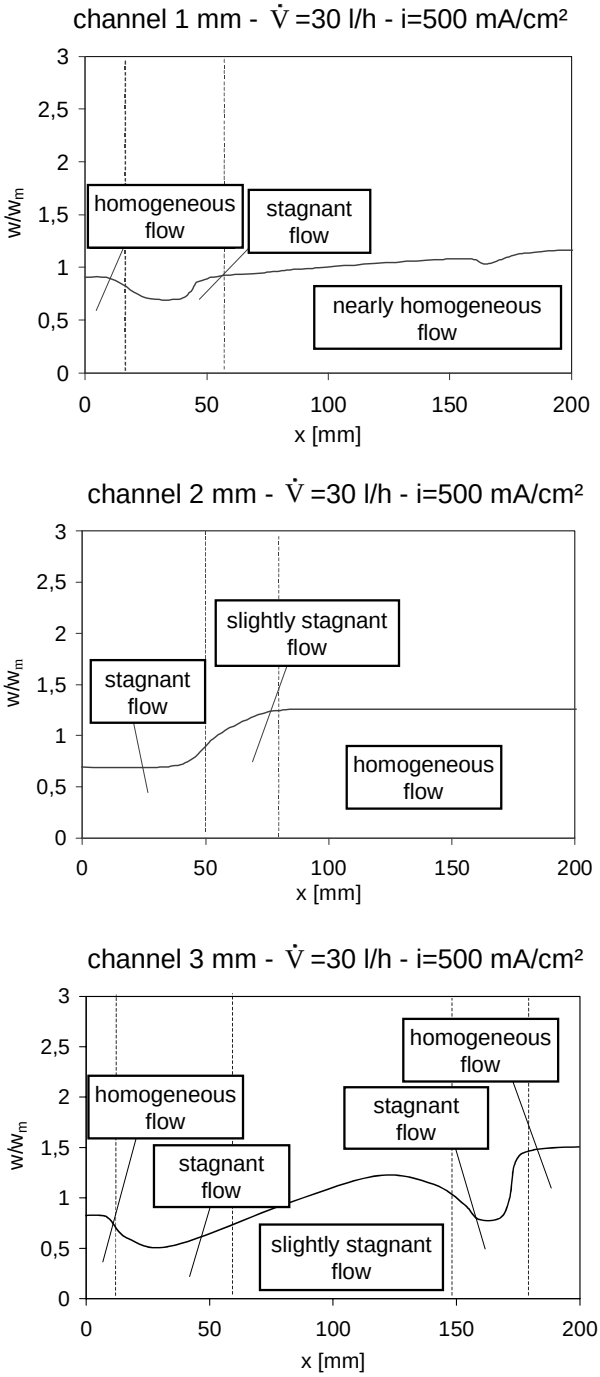

Fig. 5. Velocity and continuity of the flow: variation of flow-field design; 8.3 mm channel manifold; $\dot{V} = 30$ l/h and $i = 500\,\mathrm{mA/cm^2}$. The *x*-axis indicates the position on the width of the flow field, the *y*-axis indicates the observed velocity of the flow relative to a medium velocity.

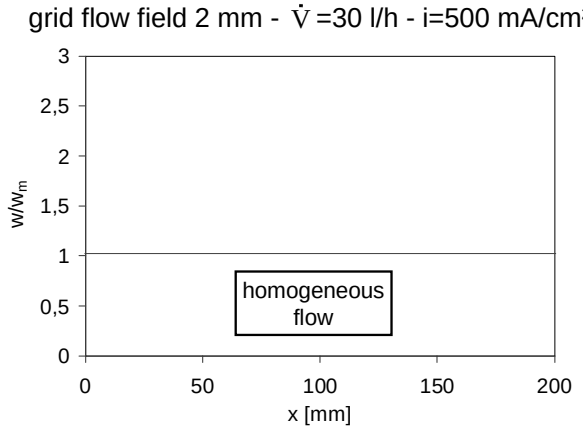

Fig. 5. (*Continued*).

3.2. Influence of manifold design on the flow homogeneity

By the new method, the suitability of various manifold designs was investigated with a 1 mm channel structure. In the experiments, the same type of manifold was used at the inlet and outlet.

The results of the two rectangular manifolds (width 3 and 8.3 mm) are similar. The flow displays similar effects for all flow parameters. Large velocity gradients in the flow structure occur particularly in the inlet and outlet region of the manifolds. This effect seems to be somewhat more pronounced for the 8.3 mm manifold channel than for a 3 mm manifold channel. In this case, the pressure fluctuation due to different gas contents in the manifold becomes apparent.

At small volumetric flows in the inlet and outlet region, due to bubble accumulation, the 3 mm manifold channel sometimes even displays a velocity minimum where theoretically a maximum should be found. At higher flow velocities and low simulated current densities, the bubbles can be removed sufficiently. In general, the velocity profile across the whole plate width is somewhat more inhomogeneous than for the 8.3 mm manifold channel.

The lack of homogeneity in the bubble discharge represents a great problem for both manifolds. The flow is stagnant over wide areas of the profiles. Although large volumetric flows can slightly improve the bubble discharge, the results are in general unsatisfactory. On the whole, the 8.3 mm manifold is superior to the 3 mm manifold.

The flow profiles shown in Fig. 6 of the splayed manifold indicate much better results than those of the rectangular manifold. In this case, the flow rate is more uniform and the bubble discharge more homogeneous. Under none of the operating conditions studied was it possible to identify any differences in the velocity of the bubbles in the anode compartment for the splayed manifold channel. The results of further studies show that it is advantageous to install splayed manifolds on the inlet and outlet side. The slight irregularities in the velocity profile in the region of the manifold inlet and outlet can only be eliminated by bigger manifold widths since this is a stagnation pressure problem caused by the inflow. This requires larger overall dimensions.

The use of grid manifolds gives a better distribution than channel manifolds, but a worse distribution than splayed manifolds. The distribution is still quite homogeneous as Fig. 7 exemplary shows for the 2 mm grid manifold.

Irrespective of variation of the manifolds, the analysis of the two-phase flow in the grid structure always displays homogeneous bubble discharge. The bubbles have a uniform velocity at each location indicating a homogeneous flow distribution.

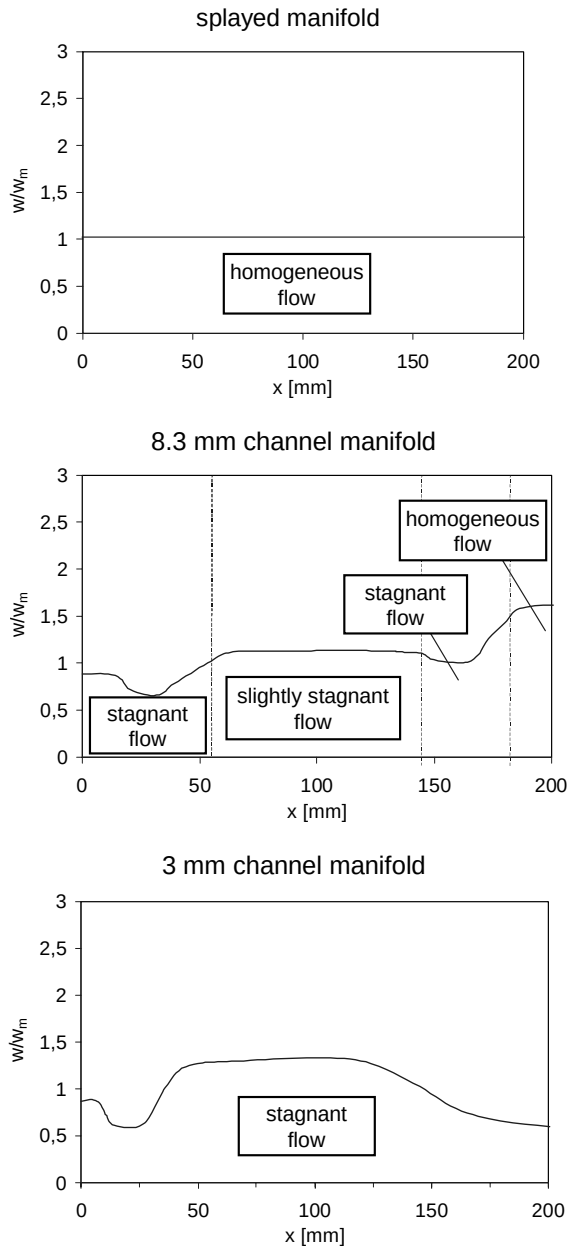

Fig. 6. Velocity and continuity of the flow: splayed manifolds, 1 mm channel flow field, $\dot{V} = 20$ l/h and $i = 500$ mA/cm^2. The *x*-axis indicates the position on the width of the flow field, the *y*-axis indicates the observed velocity of the flow relative to a medium velocity.

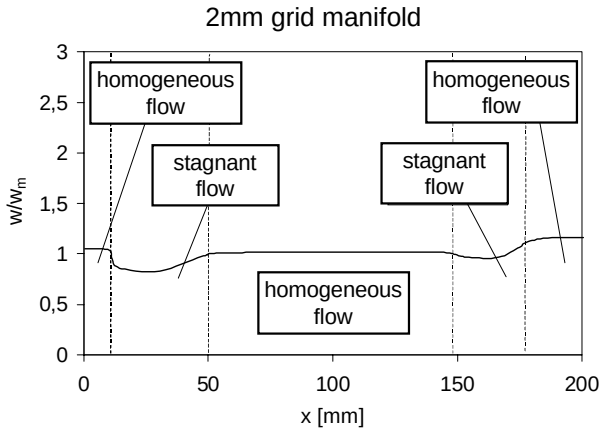

Fig. 6. (*Continued*).

Splaying the manifold encourages a more homogeneous flow rate in the respective distributor structure. As an additional observation, a minimum width (2 mm) must be ensured at the most distant point from the inlet in order to avoid clogging by bubbles. Furthermore, the manifold should not exceed a maximum width for reasons of space so that splaying it in accordance with the decrease in volumetric flow is only possible to a limited extent.

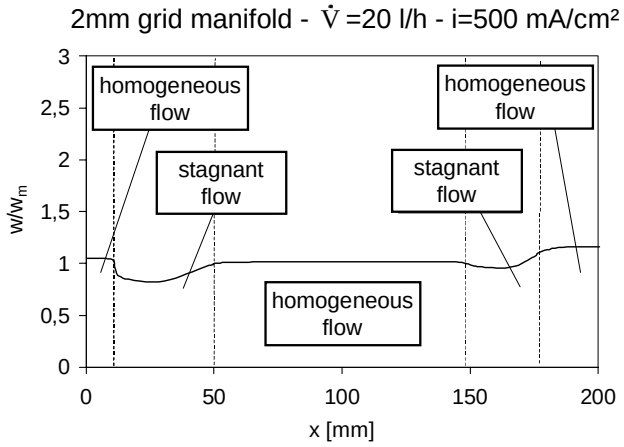

Fig. 7. Velocity and continuity of the flow: grid manifold, 1 mm channel flow field, $\dot{V} = 20$ l/h and $i = 500\,\mathrm{mA/cm^2}$. The *x*-axis indicates the position on the width of the flow field, the *y*-axis indicates the observed velocity of the flow relative to a medium velocity.

4. Summary

The newly developed method for the in situ production of gas bubbles in liquid flow can reproduce the behaviour of the two-phase flow at the anode of a DMFC. It has been established that at low volumetric flows channel structures have a tendency to inhomogeneous flows due to gas closures of individual channels. These closures can be eliminated at higher velocities in the channels due to rising pressure differences. Grid structures display good bubble discharge behaviour at all velocities and are beneficial if the flow rate should be minimised, e.g. for reasons of pump power demand. Another important criterion for two-phase flow behaviour at the anode is the suitability of the manifold for bubble discharge. Splayed manifolds show the best bubble discharge behaviour from the cell since they prevent an accumulation of gas in the manifold. Grid manifolds also display good discharge properties. Rectangular channel manifolds encounter difficulties with bubble discharge and flow homogeneity.

References

[1] K. Kordesch, G. Simader, Fuel Cells and Their Applications, VCH Verlag, Weinheim, 1996.
[2] H. Dohle, H. Schmitz, T. Bewer, J. Mergel, D. Stolten, J. Power Sources 106 (2002) 313–322.
[3] A. Kindler, T.I. Valdez, C. Cropely, S. Stone, Elect. Electrochem. Soc. Proc. 4 (2001) 231.
[4] T. Biegler, J. Electrochem. Soc. 116 (1969) 1131.
[5] W. Vielstich, Brennstoffzellenelemente, Verlag Chemie, Weinheim, 1965.
[6] H. Dohle, J. Divisek, R. Jung, J. Power Sources 86 (2000) 469.
[7] S. von Andrian, Ph.D. thesis, RWTH, Aachen, 2001.
[8] D. Thirumalai, R.E. White, J. Electrochem. Soc. 144 (5) (1997) 1717–1723.
[9] J.C. Amphlett, B.A. Peppley, E. Halliop, A. Sadig, J. Power Sources 96 (2000) 204–213.
[10] D. Epp, D. Watkins, K. Dircks, US Patent 4,988,583 (1991).
[11] K. Scott, P. Argyropoulos, A. Simoglou, W.M. Taama, in: Proceedings of the International Fuel Cell Conference, Nagoya, Japan, 1999, pp. 137–140.
[12] T. Bewer, T. Beckmann, H. Dohle, J. Mergel, D. Stolten, in: Proceedings of the First European PEFC Forum, Lucerne, Switzerland, 2001, pp. 321–330.
[13] J. Stumper, S.A. Campbell, D.P. Wilkinson, Electrochim. Acta 43 (24) (1998) 3773–3783.
[14] K. Scott, P. Argyropoulos, W.M. Taama, Electrochim. Acta 44 (1999) 3575–3584.
[15] H. Dohle, T. Bewer, WO 0221622 (2002).